SABER Algorithm Change Review

This document gives a review of the changes made to the algorithm since the initial public release of SABER data with version 1.04. Each major public release version in discussed in the following sections. An appendix is also included that gives the status of the L1B, L2A, and L2B parameters for each version.

1- V1.04

SABER operational processing began in December 2003 with version 1.04 of the processing algorithm. This is the first publicly released version of the SABER data, releasing some products: T(P), O_3 VMR from O(1-delta), O_2, OH, and NO VER. Other products such as CO_2 VMR, H_2O VMR, and O_3 VMR from the 9.6 μm channel were not yet ready for public use.

2- V1.06

Soon after the start of v1.04 production the SABER algorithm team started to work on improvements to the algorithm to address some of the remaining deficiencies. This work culminated in a new public release version (v1.06) that began production in July 2005. Major differences from v1.04 are:

Better Error handling-
Processing errors that had previously resulted in significant data lost due to failures have been eliminated. Error handling within the Level 2 processing software traps the errors, writes out a message to an error log, skips the event, and then continues on with the next event. The error logs can then be reviewed and analyzed.

Interleave averaging-
The interleave meshing technique was replaced with interleave averaging; this reduces false structure in the retrieval products.

Correction to detector memory effect-
A correction to the detector memory effect has been applied to up scans in the short-wave channels.

Correction of off-axis solar scatter in shorter wavelengths-
Scatter of solar radiation from the lower atmosphere leads to off-axis signal in the short-wave channels. This is greatly reduced in v1.06 due to improvements in the off-axis scatter removal procedure.

CO_2 line mixing-
The forward model now accounts for CO_2 line mixing using the line mixing discussed by Niro et al. [1] for channels 1-3. The impact of this is shown in Figure 1.

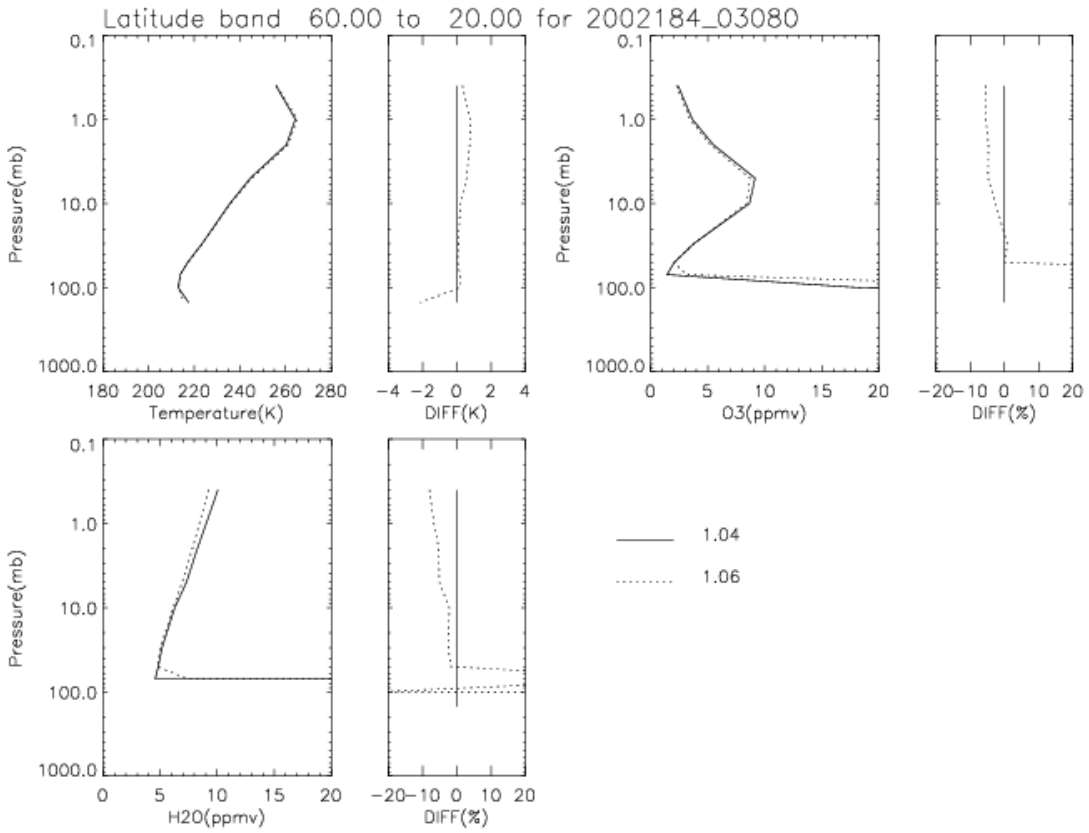

Figure 1. Impact of accounting for line mixing in the 15µm CO_2 channels.

Improved pressure registration-

Pressure registration stability has been improved by modifying the pressure range used for the registration. This was partially induced by comparisons of temperature retrieved using channel 7 vs the standard channel 3, Figure 2.

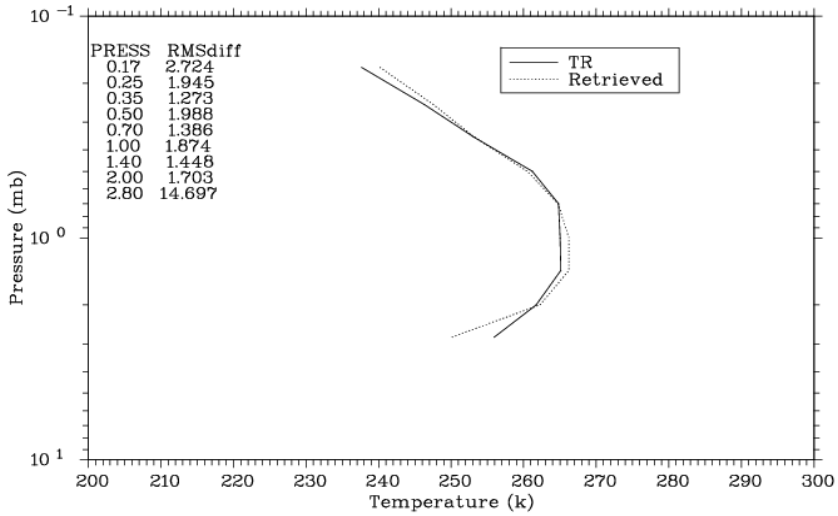

Figure 2. Comparison of T(P) retrieved from channel 7 (dotted) vs channel 3 (solid).

Updated Tvib models-
Improvements to the Curtis matrix calculation, used in the CO_2 Tvib and H_2O Tvib models, have greatly reduced failures of the retrieval.

Improved Tk resolution-
The smoothing used in the non-LTE (NLTE) Tk retrieval has been greatly reduced, increasing the resolution of the Tk profile. A 7-point 3rd degree polynomial smooth was replaced with a 3-point triangular smooth. The impact of this change is shown in Figure 3.

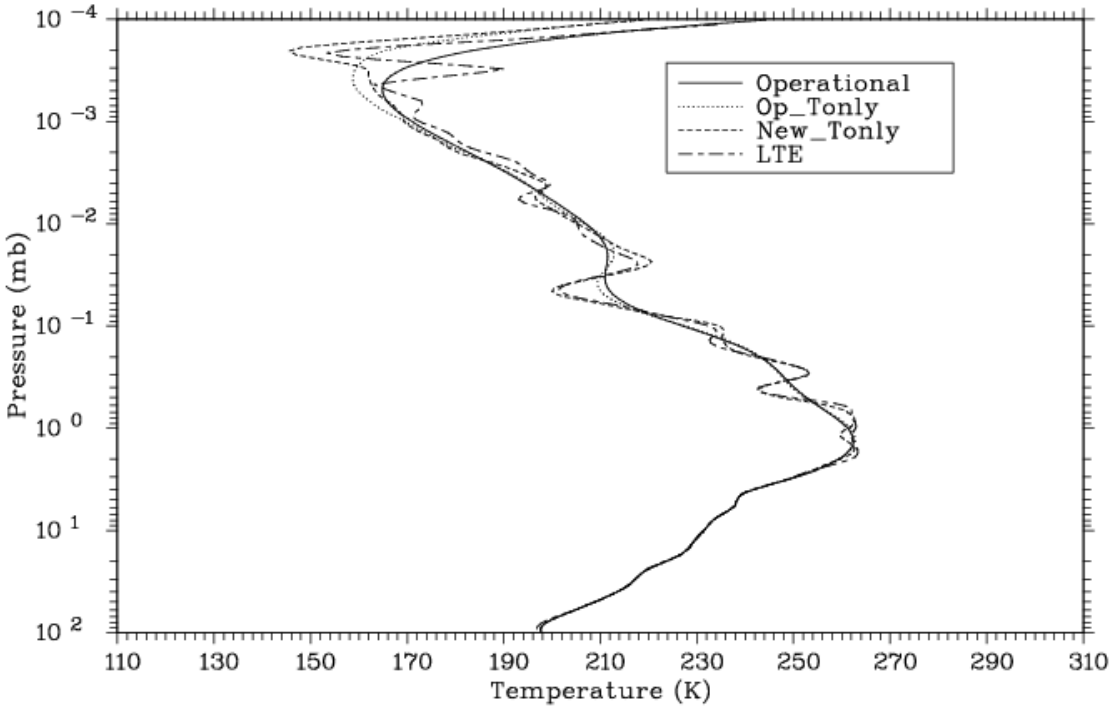

Figure 3. Impact of reduced smoothing - V1.04 (solid), V1.06 (dashed).

MSISE-90 used for O, O_2, and N_2-
MSIS-90 [2] is now used for O where not available from the new O model. In addition, N_2 and O_2 from the MSIS model are also now used.

New Unfilter Factors-
Implementation of the unfilter factors has been updated and NO now has day and night factors. OH(A) factor is 1.11 (was 1.15). OH(B) factor is 1.42 (was 1.47). $O_2(1\text{-}\Delta)$ factor is a function of T (was 1.34).

Improved Photolysis Rates-
Photolysis rates are calculated more rigorously. Daily solar flux files from SEE [3] are used for Schumann-Runge and Ly-Alpha and new Hartley fluxes are used. New cross sections used for Schumann-Runge O_2, Hartley O_3, and Ly-alpha. Also, Earth-sun distance is used to adjust solar fluxes.

O_2 Airglow Model Updated-
The O_2 airglow model has been updated with new line parameters and new radiative lifetimes for some states.

New O models-
New day/night O models are now in use. These are used for O, H, and chemical heating rates at nighttime and for O and O(1D) in daytime. Extensive screening of these products is done before their use in subsequent T, O_3, and H_2O retrievals. And MSIS-90 O is used to extend the O product in altitude for use in subsequent retrievals.

New Output products-
O_3 from 9.6 μm and daytime CO_2 are now available in the L2A files. Additional products have also been added to the Level 2B netCDF files. These include CO_2 cooling rates for selected bands, CO_2 solar heating rates for selected bands, O_2 solar heating rate for the atmospheric bands and 5 chemical heating rates.

3- V1.07

Production of v1.06 continued until a new version, v1.07, was made operational in April 2007. V1.07 improvements and differences with v1.06 are note below.

CO_2 Tvib model-
Original SABER Tvib model used in version 1.06 SOPS did not include V-V transfer between isotopes of the fundamental band (FB). V-V exchange between bands was incorrectly modelled as a thermal process. The CO_2 Tvib model was modified to properly include V-V transfer between CO_2 bands including between isotopes of the FB [4]. This corrects the SABER forward model to allow good agreement in modelled radiance verses that modelled using ALI (Accelerated Lambda Iteration) Tvibs, see Figure 4. The modified Tvib model is incorporated into the v1.07 algorithm. This has resulted in temperature cross sections that appear to be more realistic with Polar Summer mesopause about 10K warmer and at roughly 87km. Temperatures do not fall below 150K until above 80km. Also, MSIS O now used above 90km and WACCM [5] CO_2 used day and night.

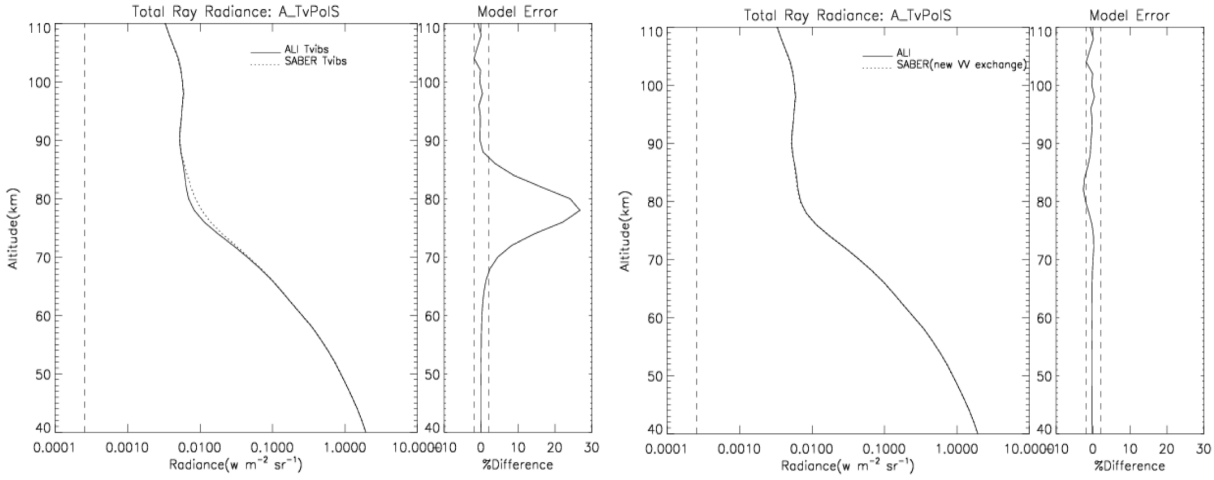

Figure 4. SABER forward model radiance comparison, Left panel ALI vibrational temperatures vs V1.06 SABER, right ALI vs v1.07 SABER.

New $O_2(1\Delta)$ VER algorithm implemented-
Both v1.06 and v1.07 use a standard Abel inversion approach for VER above 75km; this is merged with results from a strong line retrieval below 75km. However, the v1.06 strong line algorithm sometimes results in spurious data around 75km (a kink is often evident).

A new strong line algorithm is incorporated in v1.07 that calculates VER directly from the retrieved band averaged source function [6]. This eliminates the observed kinks and better matches the Abel inversion result above 75km. For version 1.07, strong line VER at the tangent point is obtained directly from the retrieved broadband average source function values:

$VER = 4\pi/hc\nu * J * d\varepsilon/ds$,

where h is the Planck constant, c is the velocity of light, ν is the band center wavenumber, ε is emissivity, and s is path length. The algorithm first retrieves tangent point J using BandPak [7] to match measured radiances. It then uses the first non-zero emissivity in the BandPak tables for the conditions of the tangent point T(P) to calculate dε/ds. This assures that the derivative is evaluated in the linear regime. HITRAN 2000 spectroscopy is now used in the strong line retrieval.

The strong line results are noisy above about 80 km and, since the lines are weak at higher altitudes, the standard Abel retrieval results are preferred above 75 km. The Abel results are for mass weighted mean along the path and must be interpolated to the tangent point for merging with the strong line results. The altitude corresponding to this mean is directly obtained from the air mass-path and it's first moment in z. These parameters are routinely supplied by BandPak. The strong line retrieved VER is merged with the interpolated Abel inversion results above 75km, Figure 5. Note that the interpolation of Abel results to the tangent point was not performed in v1.06 and the v1.06 results are typically 5% to 10% different from v1.07, Figure 6.

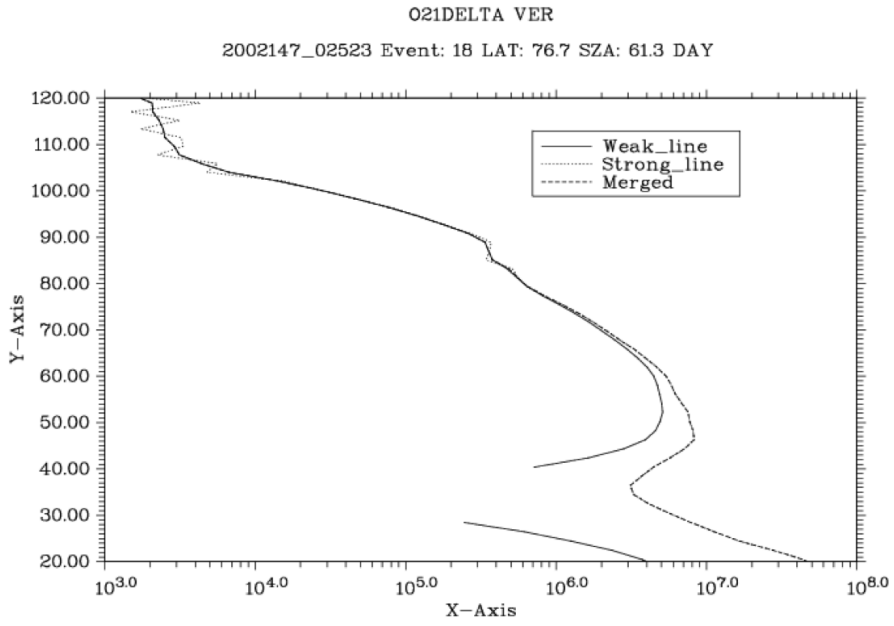

Figure 5. Example of merging weak and strong line VER.

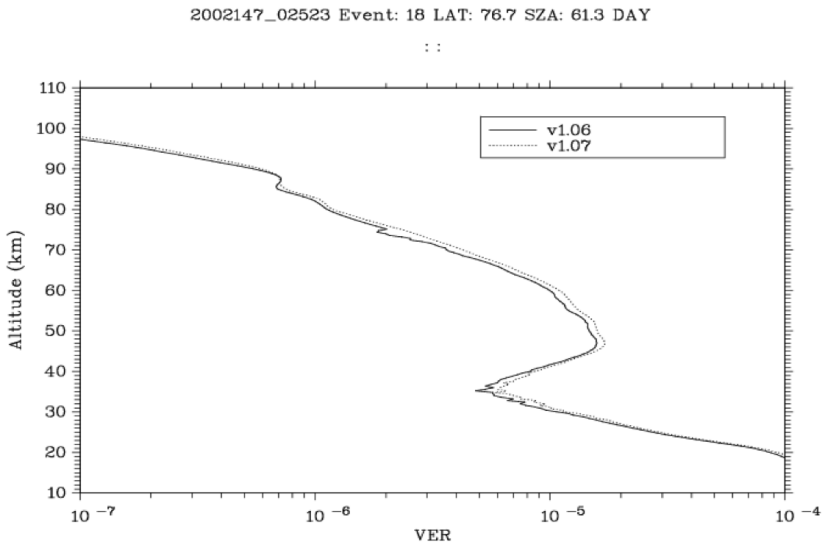

Figure 6. Comparison of v1.07 to v.1.06 VER.

MIPAS O-O_2, O-N_2 quenching rates now used in O_3 Tvib model-

O_3 retrieved from channel 4 (9.6μm) radiance data agree well with that inferred from $O_2(1\Delta)$ VER from 45-55km (LTE region). Above that altitude the two results differ significantly in version 1.06. Part of this difference is due to the use of outdated rates for quenching of O by O_2 and N_2. Contemporary temperature dependent rates from the MIPAS NLTE model [8] have been incorporated into version 1.07 SOPS. Updated code to use quasi-nascent state distribution assumption similar to that used on MIPAS. Net effect of these changes along with improvements to O_3 from $O_2(1\Delta)$ VER moves O_3 derived from 9.6μm much closer to that derived from 1.27μm below 100km, Figure 7.

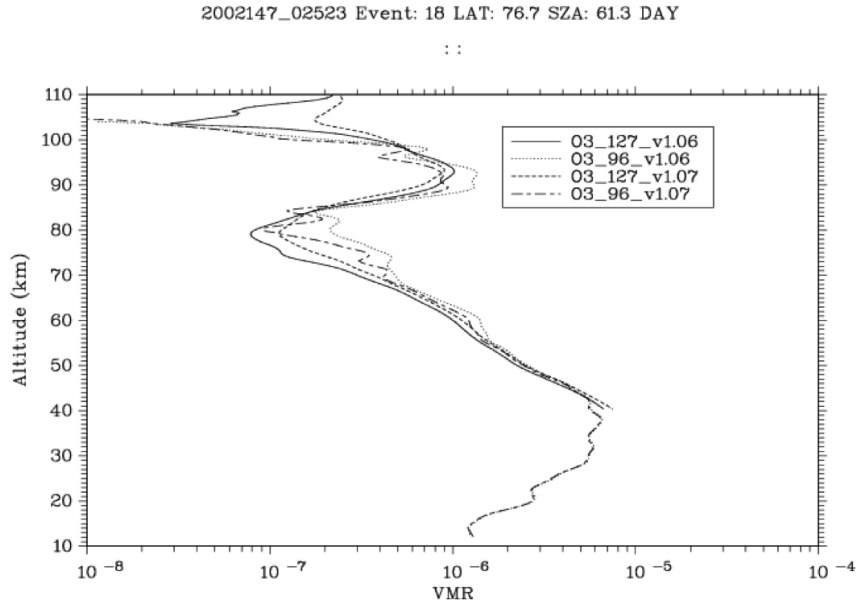

Figure 7. Comparison of v1.07 to v1.06 O_3 VMR.

H_2O product is much improved but not yet operational-
Retrieval non-linearity leads to unexpected behavior when upper altitude values are in error (errors propagate into the stratosphere). The basic H_2O NLTE model has been validated through comparisons with other groups (IAA and Goddard). Errors in the NLTE model led to upper altitude errors which propagate into the stratosphere. An error in the temperature dependence of the rate for a process ($O_2(1)+CO_2$) important to the population of $O_2(v=1)$ has been identified and corrected. This has resulted in much improved SOPS water retrievals for daytime data but still likely a 15% or so bias in the upper stratosphere/lower mesosphere. Twilight data did not include solar illumination. This has been corrected and does resolve some of the retrieval failures encountered for water. Night-time retrievals are still problematic with many failed events.

Other improvements/changes-
Replaced MSISE-90 model with NRLMSISE-00 [9]. MSIS O used at night for all processes and used during the day above 90km. SABER O is used during the day below 90km. Woods-Rottman Solar model [10] is now used for all Solar fluxes. SEE data is no longer used due to degradation of instrument and possible calibration issues. Corrected a problem with NO VER, converted VER code to double precision. Corrections and updates applied to O and H models. Corrections and updates applied to chemical energy deposition rates.

4- V2.0

Production of v1.07 continued until January 2013, 2 months after a new version (v2.0) started production in November 2012. V2.0 incorporated many improvements over v1.07. The v2.0 algorithm has many improvements over v1.07 in both the Level 1 procedures, which turn the instrument data into calibrated radiance profiles, and Level 2 procedures, which produce the science products from the Level 1 radiance data. The level 1 improvements are primarily in the correction of electronic gain steps and corrections to detector relaxation of the long-wave channels (1-7) for the up scans. These improvements reduce up-down scan differences that were evident in v1.07 to residual levels that are essentially insignificant.

4.1- Level 1 Improvements

Gain correction -
In early 2009 researchers noticed a scan mode difference in the SABER temperature and water products. The left panel of Figure 8 shows an example for temperature - note the horizontal features at roughly 55 to 60km and 40 to 45km. These features were traced to error in knowledge of the electronic gain step. That error can range from several tenths percent to several percent, depending on gain mode and channel. This was investigated 3 ways: 1- analyzing the entire SABER dataset for channels 1-7, 2- using a detailed examination of slow scan events taken on January 24, 2004, for channels 1-10, and 3- examination of a special scan sequence performed on October 30, 2009, that viewed the internal baffles and the IFC for channels 5-7. The first two analyzes were consistent for channels 1-4 and the latter two for channels 5-7, channels 8-10 were only analyzed using the slow scan. The final gain steps were taken from the slow scan analysis. As seen in the right panel of Figure 8, use of these gain steps eliminates the horizontal features seen in the left panel. Note that even after the gain corrections are applied there are still residual differences between up and down scan modes. This may be due to detector relaxation effects for the up scan.

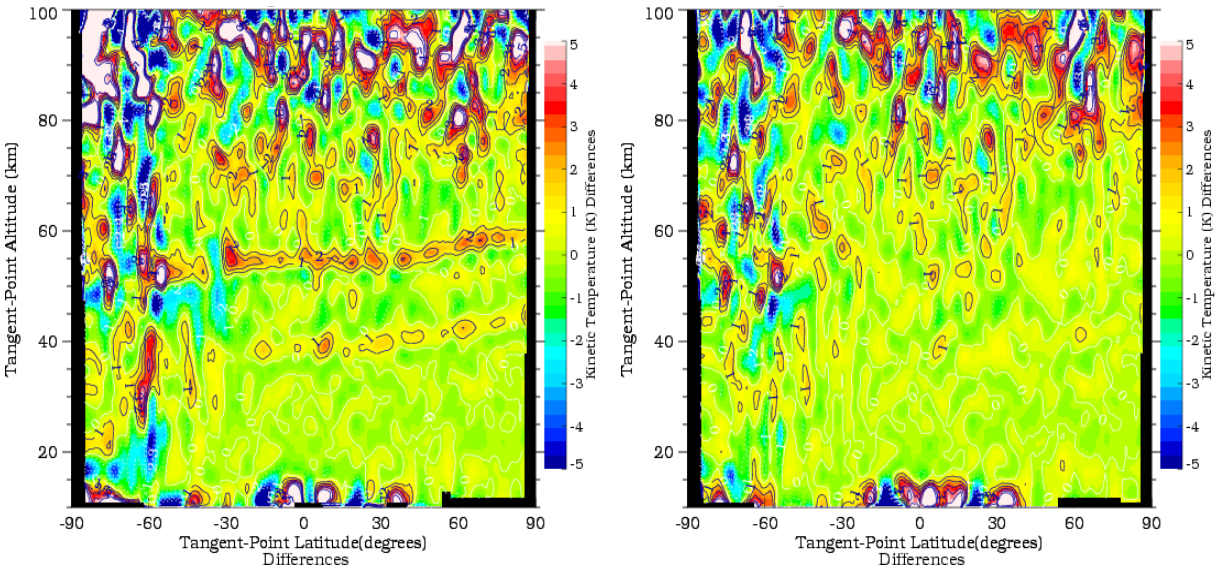

Figure 8. Up-down mode difference in temperature for July 15, 2004, left panel v1.07 SABER, right v2.0.

Detector Relaxation –
Residual up-down differences in the long wave channels are very likely due to detector relaxation effects. Detector relaxation is a known problem for some of the channels during the up-scan measurement mode. It is caused by relaxation time of the detector to input signal. Scanning from high signal toward low signal can be a problem due to the scan rate being too fast for the detector to relax from the high signal input. This problem is particularly bad for the shortwave channels (8-10) and those channels have been corrected for this since the first data release. Until recently it had not been thought that the longer wave channels (1-7) were sufficiently impacted to warrant correction. However, with the recent attempt to make water an operational product, water was found to have an up-down mode difference that is very likely caused by detector relaxation. Temperature and ozone also appear to have significant, though relatively small up-down mode differences as well. In 2011 we investigated correcting this by applying a similar approach as was used for the shortwave channels. This approach involves determining coefficients, **a** and **b**, for use in a signal correction, C, based on an exponential time decay function. That is, for each time, t(i), determine a correction coefficient:

$$C(t(i)) = \mathbf{a}\sum N(t(j))\exp(\mathbf{b}(t(i)-t(j))),$$

where N is signal and the summation is over j=0,i-1. Practical application requires analysis of a large set of up and down scans to derive the **a** and **b** coefficients and then applying the derived time decay function to each up-scan event. This procedure has been implemented and is operational in v2.0. Impact on retrieved temperature are shown in Figure 9, note that the spikes at about 45 and 60 km for the v1.07 data are due to errors in gain correction. The small (2 K) difference in the 80 – 90 km region is greatly reduced with the application of detector relaxation correction.

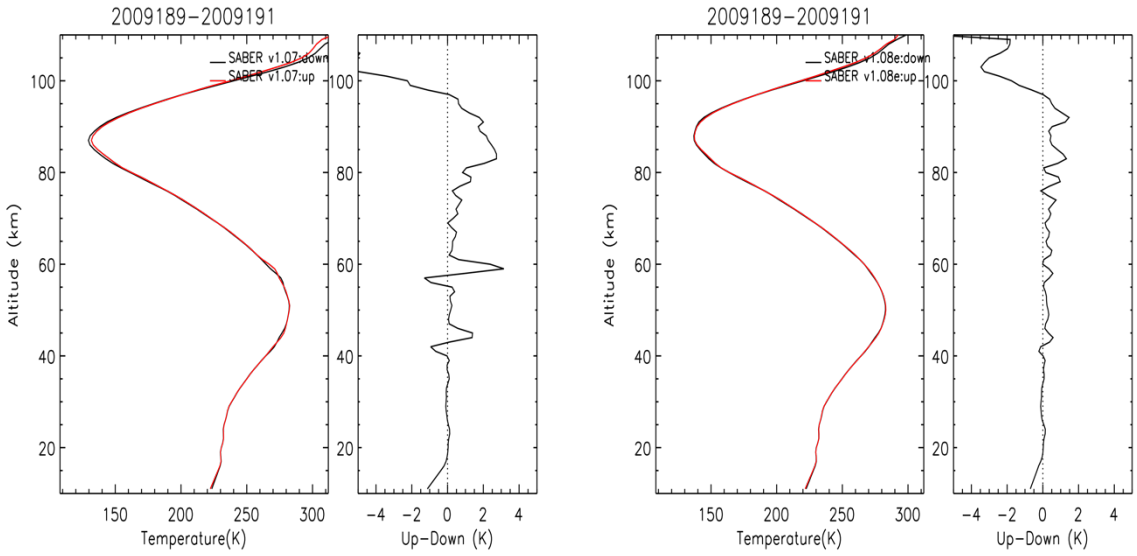

Figure 9. Average up – down node differences for July 8-10, 2009, left v1.07, right v1.08e (preliminary v2.0) , which includes detector relaxation correction.

FOV extension -

Another area of investigation is the FOV function in the far wings. Laboratory data was only usable in the vicinity of the main FOV lobe and first side lobe (and for some channels the second side lobe). The remainder of the FOV function was not adequately characterized during ground calibration. In 2003 and 2004 this was corrected using a sequence of lunar scans that helped define the wings of the FOV function. That data resulted in much better defined FOV functions past the first side lobe. Due to limitations in that procedure the functions past about 1 degree from center were still not well characterized, but since the response at that point was typically below 1e-5 it was thought at the time that the functions would be adequate. However, further analysis for channel 4 and 5 suggested that error in FOV function past 1 degree from center can contribute significantly to error in the ozone and water retrieval products in the mesosphere. The FOV functions were extended out to 2.5 degrees from center using a function estimated from BRDF curves for the scan mirror. Figure 10 shows laboratory (solid black line) and most recent corrected FOV (dashed red line) for channel 1.

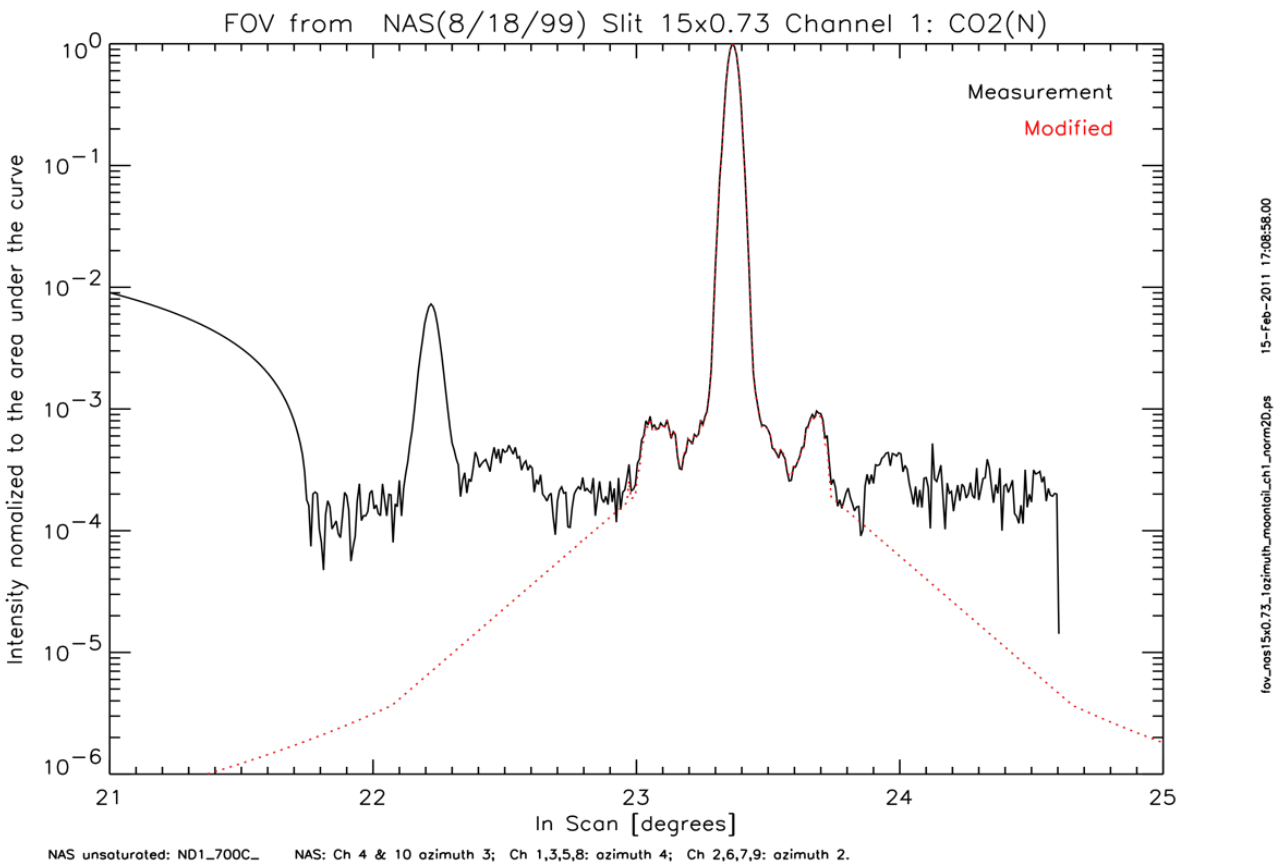

Figure 10. SABER FOV functions for channel 1, solid black is the laboratory calibration curve and dashed red is the curve used in the v2.0 algorithm.

Radiance Offsets –
Due to internal emission for the long-wave channels changing as a function of scan angle, SABER cannot use the space look signal to determine offsets. Therefore, a search of the limbpath data is made for the altitude region of lowest observed signal and the offset is determined from an average over that region. While investigating the far off-axis FOV functions, it was determined that the signal minimization procedure used for determining the offsets did not allow for the full range of expected conditions (low solar activity to solar storm) for some channels. A new procedure was implemented to correct this and to correct an error that allowed the space look signal to be used as offset for events that did not have sufficient data to determine a signal minimum. Figure 11 shows the average signal to noise profiles for each channel for June 30, 2009, note the increasing signal with increasing altitude for most of the long-wave channels, most notably channels 4 and 5.

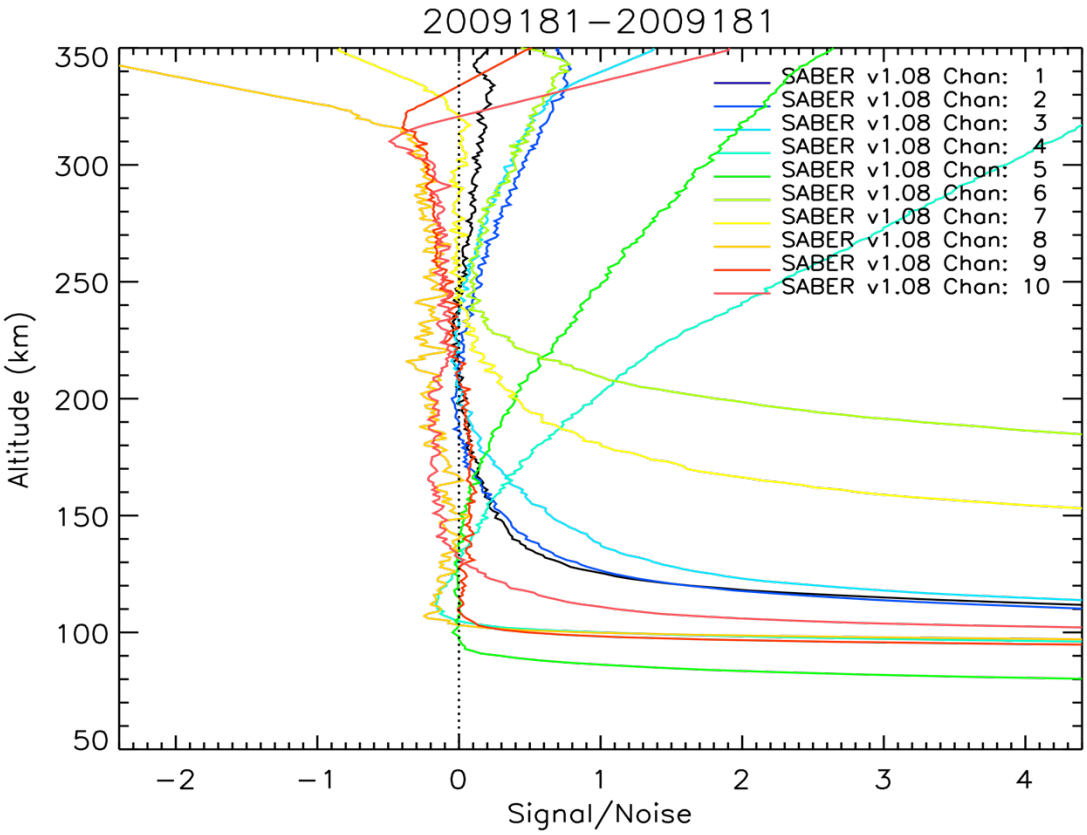

Figure 11. Average signal to noise profile for each channel for June 30, 2009, notice that most long-wave channels appear to have an offset that varies with altitude.

4.2- Level 2 improvements

Level 2 improvements are primarily in the procedures used to simultaneously retrieve temperature and pressure in the middle stratosphere - where the CO_2 populations of interest are in local thermodynamic equilibrium (LTE), and to the procedures used to retrieve temperature for conditions that are not in local thermodynamic equilibrium (NLTE) - primarily involving details of the vibrational temperature model iteration and maintenance of input parameters as functions of pressure.

T(P) Improvements-
The simultaneous retrieval of temperature and pressure uses at least 2 CO_2 channels that have significantly different responses to changes in pressure. The current algorithm uses channels 1 (narrow band CO_2) and channel 3 (one of 2 wide-band CO_2 channels). In the past we've investigated use of all three CO_2 channels and various configurations of altitude ranges over which these channels are used. The v1.07 algorithm (which also uses channels 1 and 3) implemented a forward model switch at 50km that could lead to a significant discontinuity at 50 km. We've modified the procedure to eliminate such forward model switches and implemented other less significant modifications in an attempt to improve performance for the difficult high latitude winter situations.

We've also taken another look at the rate used for VV exchange between v2 isotopes. Based on the work of Kutepov et al. [4] for v1.07 SABER we used 2.4e-11 for the exchange rate for the fundamental band and 1.2e-11 for the first hot band. Subsequent work by the IAA group determined that the same rate should have been used for both bands and that rate should be in the range of laboratory measurements (1.2e-11 to 2.4e-11). Further discussion led to testing of 2 settings: 1) a median value of 1.8e-11 and 2) the higher rate of 2.4e-11 used on MIPAS and recommended for use on SABER. In the course of investigating these settings we also tested sensitivity to number of iterations used in the vibrational temperature model, v1.07 used 2 iterations to save time but in some situations 3 iterations are needed. Figure 12 shows the impact of each of these settings on the retrieval of a single polar summer event. This figure shows the retrieval of T(P) using each of these options and for comparison the results from version 1.07, and the falling sphere climatology of Lubken [11]. The VV rate has large impact above about 79km and the number of iterations impacts results in the 79-84 km region. Baseline for v2.0 is the 2.4e-11 rate using 3 iterations.

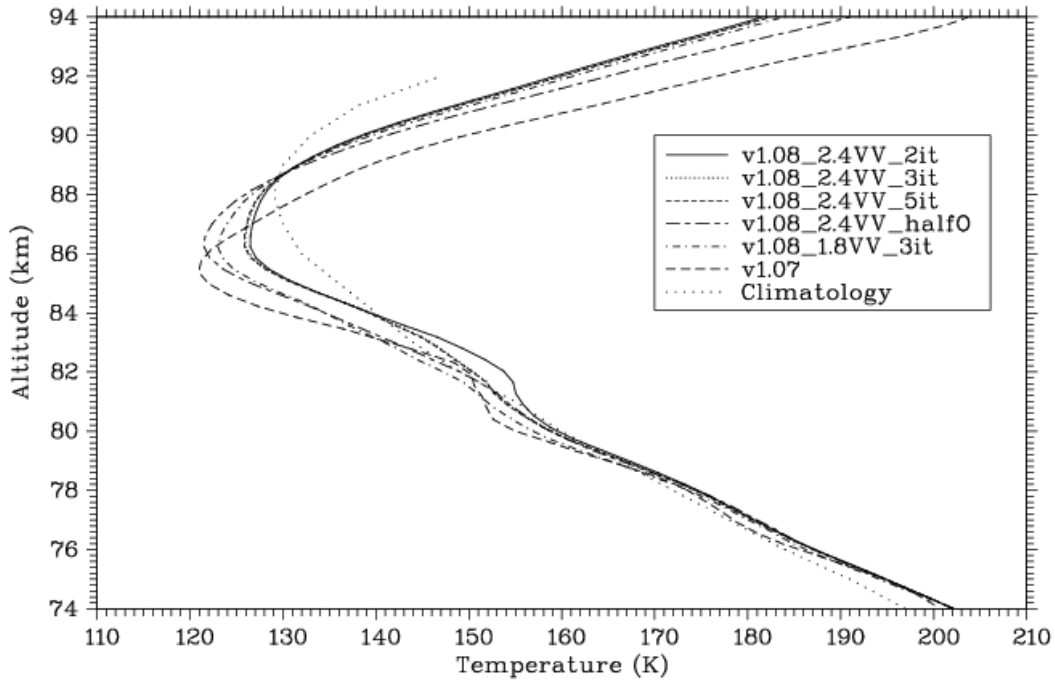

Figure 12. Impact of VV exchange settings on a polar summer event.

Also shown in Figure 12 is the impact of 50% reduction in atomic oxygen O(3P). The v1.07 algorithm uses SABER derived O(3P) for daytime but the NRLMSIS-00 model results for twilight and nighttime. Figure 13 shows impact of O(3P) VMR profile on retrieved T(P) for a single event from July 2, 2002. Comparisons of polar summer coincidence data for terminator events for SABER, SOFIE, and ACE (Figure 14) suggest that results derived from the SABER daytime airglow model should be used in T(P) retrieval for twilight. The v2.0 algorithm was modified to use daytime code to derive O for twilight conditions and to use this derived O in the T(P) retrieval for both day and night.

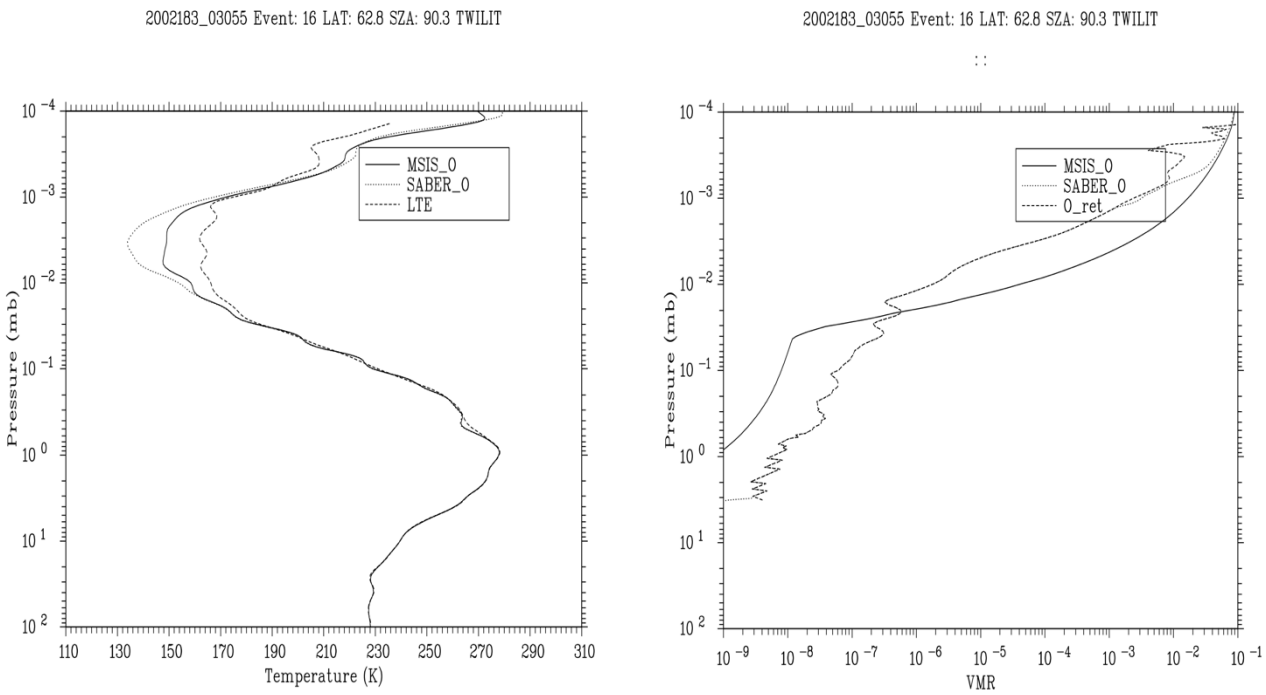

Figure 13. Impact of O(3P) on retrieved T(P), left panel temperature, right O(3P) VMR.

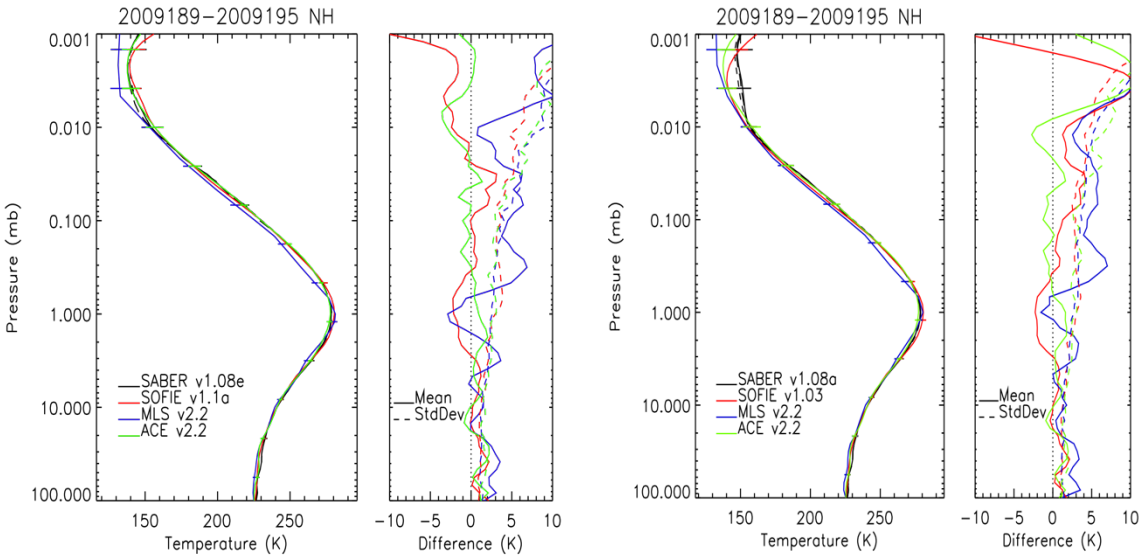

Figure 14. SABER comparisons to SOFIE, ACE, and MLS, left using SABER derived O(3P), right using NRLMSIS-00 O(3P).

The T(P) retrieval improvements along with significant changes to the climatology (now using WACCM 3.5.48) have greatly reduced the number of rejected events (and anomalies), particularly for the problematic polar winter periods. Figure 15 provides a good example of this improvement, it compares the rejection frequency for the NH winter yaw period, January 11 to March 15, 2009, a period that includes a strong sudden stratosphere warming (SSW) event - note the dramatic reduction in rejected events for the NH polar region. Anomalies still occur with v2.0 and to improve identification of such events, we have

implemented improvements to the screening algorithm. The most powerful screens are (1) comparisons of LTE retrieved to NLTE retrieved T(P) in an altitude region where these should give very close to the same result and (2) interleave to interleave variations.

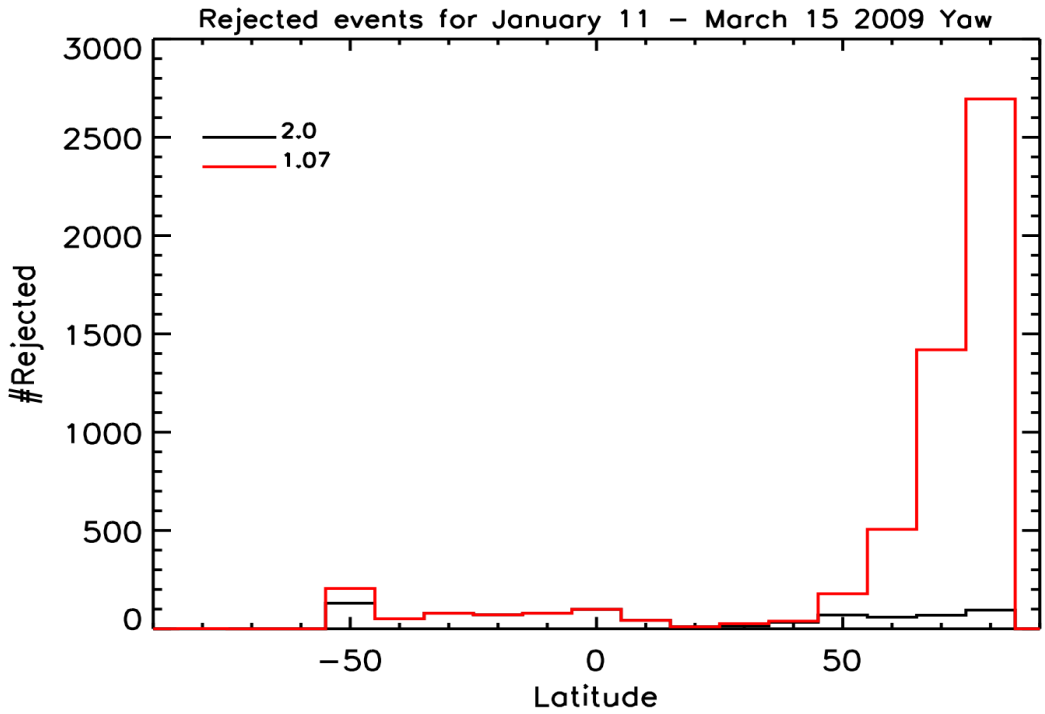

Figure 15. Rejected events for v2.0 vs v1.07.

Ozone and water –
Biases in ozone and water still remain in v2.0. Though ozone from the 9.6 µm channel appears to have biases ranging up to as much as 15% it has proven to be useful for research and the new version is more self-consistent with results from the airglow channel. Water was not yet of high enough quality to be released with v2.0, though it is released with a revised algorithm in 2019.

Channel 7: 4.3 µm CO_2 –
Small errors in the CO_2 vibrational temperatures (Tvibs) can lead to large errors in modeled channel 7 radiance. Figure 16 compares the radiance profile computed for the bands used by SOPS and using the Tvibs generated by the SOPS code to that using Tvibs generated for the same levels by an independent accelerated lambda iteration code (ALI-ARMS). As can be seen from this plot, the radiance differs by as much as 15% in the upper mesosphere. Furthermore, recent work by Ladi Rezac from HU suggests that several additional isotopic hot bands need to be included in the SOPS algorithm to correct radiance by another 5%+ in the middle mesosphere. Further progress on the SOPS CO_2 VMR retrieval cannot be made until these issues are resolved. Hampton University researchers continued this work and as noted below, have achieved a reliable CO_2 VMR retrieval using an independent algorithm as a post-process. However, the v2.0 operational algorithm does not output the CO_2 VMR product.

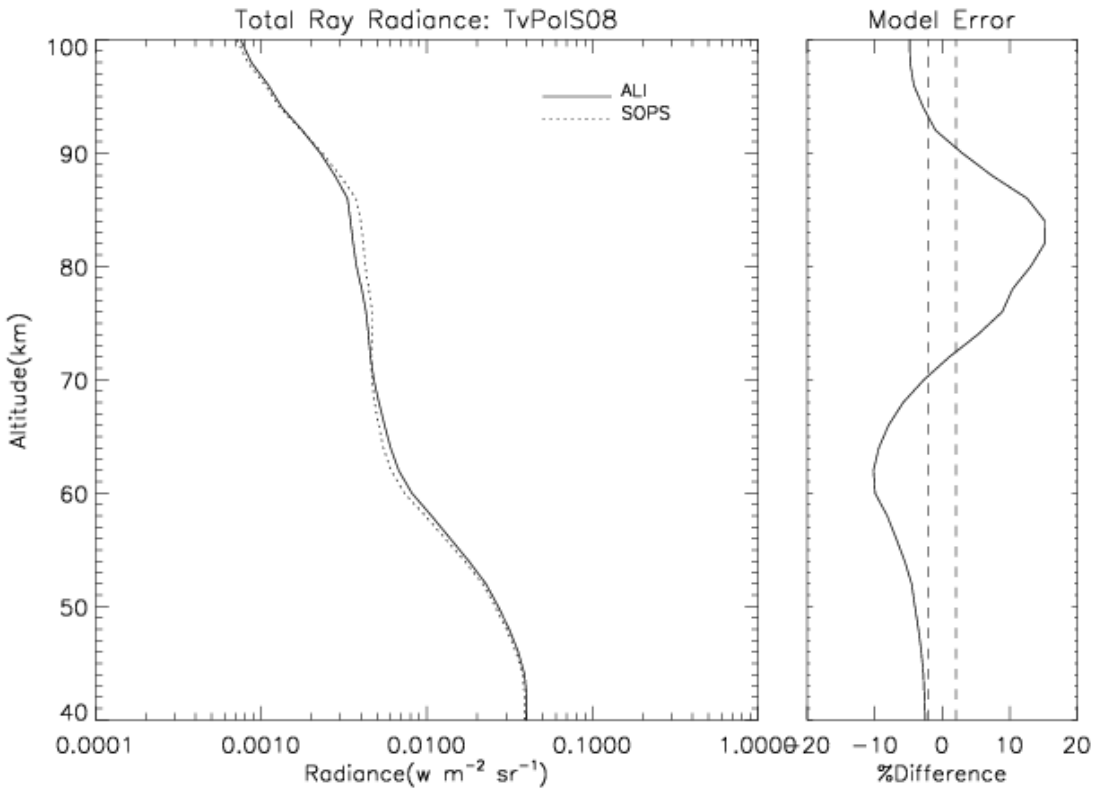

Figure 16. Channel 7 (4.3 μm) radiance difference using SOPS Tvibs vs. ALI-ARMS Tvibs.

Other improvements-
The v2.0 level2 algorithm also includes significant improvements to the O, H, and chemical heating algorithm, primarily updated reaction rates and procedures and a final pass calculation of energetics parameters.

In addition to the v2.0 algorithm, a separate algorithm was developed and implemented by HU in 2015 to simultaneously retrieve temperature and CO_2 mixing ratio from ~70 - 125km altitude. This algorithm uses the ALI-ARMS RT code that corrects the deficiencies of the SOPS 4.3 μm CO_2 vibrational temperature model noted above, see Rezac et al [12]. These data have been made available to the public as a separate product.

5- V2.0x

The version 2.0 algorithm has undergone some revision over the years since its initial release. The major revisions are noted below.

Change to account for orbit degradation-
The algorithm was modified in October 2016 to account for the slow degradation of the TIMED orbit. The orbit degradation had gotten to the point that it interfered with the calculation of radiance offsets for

the NO channel (using high tangent altitude measurements). This issue resulted in numerous event failures from mid 2015 (missing a few tropical events per orbit) to October 2016 (missing most NH tropical events). The last failure of this sort occurred October 9, 2016. Data for dates beyond this have been processed using the modified code. All of the missing data from 2015 and 2016 have been restored and merged into new netCDF files (designated v2.01) for all orbits that contain missing events. Diagnostics were added to facilitate monitoring of orbit degradation on SABER processing. These diagnostics confirm that the code modifications are properly handling the orbital changes without impacting the science data and should do so until at least 2027.

H_2O-
In March 2019 the H_2O parameter was released as a public product. This was accomplished by correction of a suspected out-of-band spectral response leak in the H_2O channel from the 9.6 ozone band [13]. These data are produced as a post-process of the v2.0 data and merged into a new version, 2.07, of the netCDF files. These files are identical in every way to the v2.0 files except for the newly released H_2O parameter. Version 2.07 is the version currently served to the public.

Impact of WACCM input –
V2.0 SABER processing uses a version of WACCM, 3.5.48, that is no longer supported. The WACCM 3.5.48 input file used by SABER processing extended through 2019 and on December 15, 2019, a switch was made to WACCM 4. The primary use of the WACCM input is setting of the CO_2 VMR profile used in the T(P) retrieval. This switch to WACCM 4 included a change to the CO_2 profile shape in the thermosphere (a more rapid fall off in VMR with increasing altitude as shown in Figure 17) which impacts the T(P) retrieval above about 90 km. We have reprocessed the SABER data from December 15, 2019, to present using a CO_2 consistent with WACCM 3.5.48. The netCDF data files for this reprocess are designated as version 2.08 to distinguish them from the existing 2.07 files. Going forward, the production files will also be designated as version 2.08. Data through December 14, 2019, are still designated as v2.07.

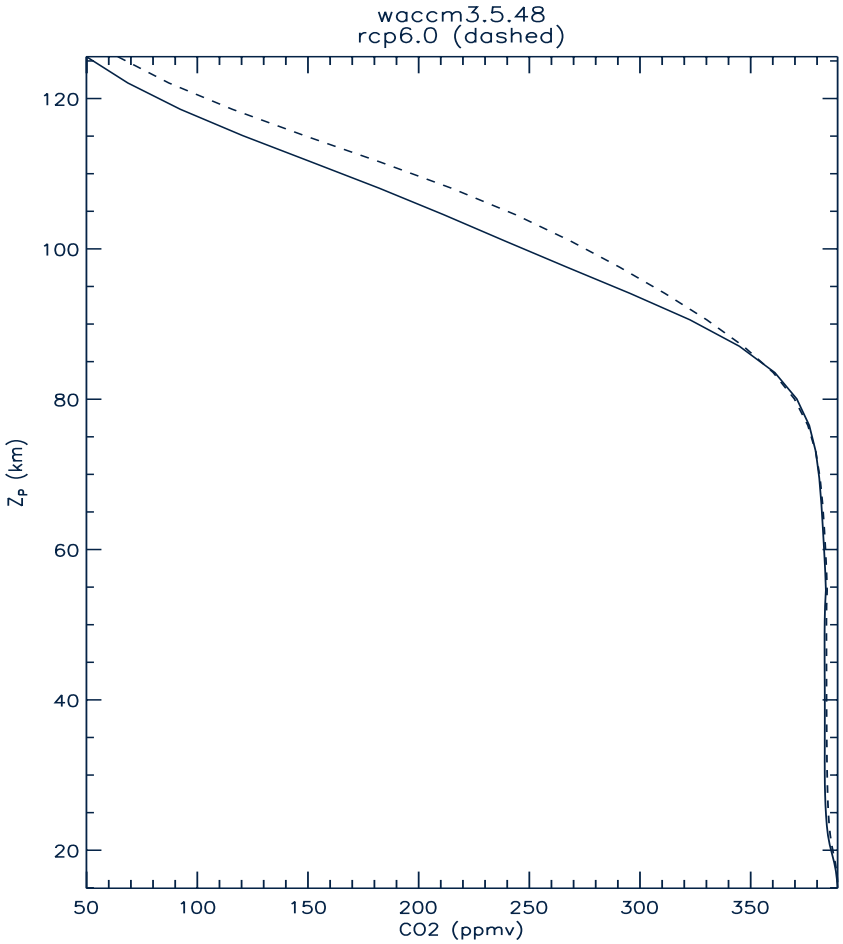

Figure 17. WACCM CO_2 solid - version 3.5.48, dashed - version 4.

References

1. Niro, F., T. von Clarmann, K. Jucks, and J-M. Hartmann (2005), Spectra calculations in central and wing regions of CO_2 IR bands between 10 and 20 μm, III: atmospheric emission spectra, *J. Quant. Spectrosc. Radiat. Transfer*, **92**, 61-76.
2. Hedin, A. E. (1991), Extension of the MSIS Thermosphere Model into the middle and lower atmosphere, *J. Geophys. Res.*, **96** (A2), 1159– 1172, doi:10.1029/90JA02125.
3. Woods, T., F. Eparvier, S. Bailey, P. Chamberlin, J. Lean, G. Rottman, S. Solomon, W. K. Tobiska, D. Woodraska, (2005). Solar EUV Experiment (SEE): Mission overview and first results. *J. Geophys. Res*. (Space Physics), **110,** 1312-. 10.1029/2004JA010765.
4. Kutepov, A. A., A. G. Feofilov, B. T. Marshall, L. L. Gordley, W. D. Pesnell, R. A. Goldberg, and J. M. Russell III (2006), SABER temperature observations in the summer polar mesosphere and lower thermosphere: importance of accounting for the CO_2 ν_2 quanta V-V exchange, *Geophys. Res. Lett.*, **33**, L21809, doi:10.1029/2006GL026591.
5. Garcia, R. R., D. R. Marsh, D. E. Kinnison, B. A. Boville, and F. Sassi (2007), Simulations of secular trends in the middle atmosphere, 1950-2003, *J. Geophys. Res*., **112**, D09301, doi:10.1029/2006JD007485.

6. Mlynczak M. G., B. T. Marshall, F. J. Martin-Torres, J. M. Russell III, R. E. Thompson, E. E. Remsberg, L. L. Gordley (2007), Sounding of the Atmosphere using Broadband Emission Radiometry observations of daytime mesospheric $O_2(^1\Delta)$ 1.27 μ m emission and derivation of ozone, atomic oxygen, and solar and chemical energy deposition rates, *J. Geophys. Res*., **112**, D15306, doi:10.1029/2006JD008355.
7. Marshall, B. T., L. L. Gordley, and D. A. Chu (1994), Bandpak: algorithms for modeling broadband transmission and radiance, *J. Quant. Spectrosc. Radiat. Transfer*, **52**, 581-599.
8. Funke, B., M. López-Puertas, M. García-Comas, M. Kaufmann, M. Höpfner, and G. Stiller (2012), GRANADA: A Generic RAdiative traNsfer AnD non-LTE population algorithm, J. *Quant. Spectrosc. Radiat. Transfer*, **113**, 1771–1817, doi:10.1016/j.jqsrt.2012.05.001.
9. Picone, J.M., A. E. Hedin, D. P. Drob, A. C. Aikin (2002), NRLMSISE-00 empirical model of the atmosphere: Statistical comparisons and scientific issues, *J. Geophys. Res.*, **107** (A12), Pages SIA 15-1-SIA 15-16, doi:10.1029/2002JA009430.
10. Woods, T., G. Rottman (2002), Solar Ultraviolet Variability Over Time Periods of Aeronomic Interest, Washington DC American Geophysical Union Geophysical Monograph Series, 10.1029/130GM14.
11. Lubken, F. J. (1999), Thermal structure of the Arctic summer mesosphere, J. Geophys. Res., **104**, 9135–9149.
12. Rezac, L., A. Kutepov, J. M. Russell III, A. G. Feofilov, J. Yue, and R. A. Goldberg (2015), Simultaneous retrieval of T(p) and CO2 VMR from two-channel non-LTE limb radiances and application to daytime SABER/TIMED measurements, *J. Atm. And Solar-Terrestrial Physics*, 130-131, 23– 42.
13. Rong, P. P., J. M. Russell, B. T. Marshall, L. L. Gordley, M. G. Mlynczak, and K. A. Walker (2019). Validation of water vapor measured by SABER on the TIMED satellite, *J. Atmos. Sol. Terr. Phys*., doi:10.1016/j.jastp.2019.105099.

Appendix: SABER NetCDF file parameter review

Table A.1 describes the contents of the SABER L1B NetCDF files. This table lists each variable contained in the netCDF file along with its type, dimensions, units, long name, and missing value. The L1B dimensioning variables are: Channel=10, elevation=1401, pressure_nmc=64, vector=3, str_len=6, event=UNLIMITED. The event dimension will depend on the number of events in the netCDF file. Note that 3 public versions of the Level1B files have been processed: version 1.04 (used for processing version 1.06 L2), 1.07 and 2.0.

Table A.1. Level 1B variables.

variable(dimensions)/type*	Units	Long name	Missing value	Version**
ChannelName(channel,str_len)/c				04 07 20
sigma(channel)/f				04 07 20
event(event)/s		Event Number for Current File	-9	04 07 20
preEvent(event)/s		Previous event indicator	-9	04 07 20
date(event)/i		Date [yyyyddd]	2001100	04 07 20
mode(event)/s		Mode (0=Down 1=Up)	-9	04 07 20
tpDN(event)/s		Tangent Point Day/Night (0=Day 1=Night,2=terminator (85<solar zenith angle<95))	-9	04 07 20
tpAD(event)/s		Tangent Point Asc/Des (0=Ascending 1=Descending)	-9	04 07 20
offsetALT(event)/f	km	Altitude offset from Level2	0	04 07 20
twistAngle(event)/f	degrees	Residual Twist Angle	0	04 07 20
motionFactor(event)/f		Residual Motion Scale Factor	1	04 07 20
moonSepAngle(event)/f	degrees	Separation Angle (los & moon)	-999	04 07 20
tpaltmoonSepAngle(event)/f	km	Tp Altitude at Separation Angle	-999	04 07 20
solAP(event)/f		Solar Ap Index	-9	04 07 20
solKP(event)/f		Solar Kp Index	-9	04 07 20
solf10p7Daily(event)/f		F10.7 Flux (Daily	-999	04 07 20
solF10p781dAvg(event)/f		F10.7 Flux (81-day Average)	-999	04 07 20
solSpotNo(event)/s		Zurich Sunspot Number	-9	04 07 20
scSolarZen(event)/f	degrees	Sc solar zenith angle	-999	04 07 20
earth_sun(event)/f	km	Earth-Sun distance	-999	04 07 20
lunar_vector(event,elevation,vector)/f		Vector to center of moon from spacecraft	-999	04 07 20
pressure_nmc(event,pressure_nmc)/f	mbar	NMC pressure at TP	-999	04 07 20
temperature_nmc(event,pressure_nmc)/f	K	NMC temperature at TP	-999	04 07 20
geopotential_height_nmc(event,pressure_nmc)/f	km	NMC Geopotential Height		04 07 20
time(event,elevation)/i	msec	Time since midnight (UT)	-999	04 07 20
sclatitude(event, elevation)/f	degrees(N)	Spacecraft latitude	-999	04 07 20
sclongitude(event, elevation)/f	degrees(E)	Spacecraft longitude	-999	04 07 20

scaltitude(event, elevation)/f	km	Spacecraft altitude	-999	04 07 20
tplatitude(event, elevation)/f	degrees	Tangent point latitude	-999	04 07 20
tplongitude(event, elevation)/f	degrees	Tangent point longitude	-999	04 07 20
tpaltitude(event, elevation)/f	km	Tangent point altitude		04 07 20
tpSolarZen(event, elevation)/f	degrees	Tangent point Solar Zenith Angle	-999	04 07 20
tpSolarLT(event, elevation)/f	msec	Tangent point local solar time***	-999	04 07 20
elevation(event, elevation)/d	milliradian	Elevation Angle	-9999	04 07 20
scanAng(event, elevation)/d	milliradian	Mirror Scan Angle	-999	04 07 20
Rad(event, elevation, channel)/f	Watts/m2/sr	Calibrated Radiance	-999	04 07 20
scattitude(event, elevation, vector)/f	degrees	Spacecraft attitude vector	-999	04 07 20
maxRate(event)/f	degrees/sec	Maximum scan rate		04 07 20
timeMaxRate(event)/i	msec	Time corresponds to maximum scan rate		04 07 20
angleMaxRate(event)/f	degrees	Angle corresponds to maximum scan rate		04 07 20
qaRelaxationCorr(event, channel, vector)/f		QA for Relaxation Correction in Corrected Radiance	-999	04 07 20
qaRelaxationPctg(event, channel, vector)/f		QA for Relaxation Correction in Percent Total Radiance	-999	04 07 20
qaScatterCorr(event, channel, vector)/f		QA for Scatter Correction in Corrected Radiance	-999	04 07 20
qaScatterPctg(event, channel, vector)/f		QA for Scatter Correction in Percent Total Radiance	-999	04 07 20
tplatdeltaA(event, elevation)/f	degrees	Tangent Point Latitude Gradient Near Side	-999	20
tplondeltaA(event, elevation)/f	degrees	Tangent Point Longitude Gradient Near Side	-999	20
tplatdeltaB(event, elevation)/f	degrees	Tangent Point Latitude Gradient Far Side	-999	20
tplondeltaB(event, elevation)/f	degrees	Tangent Point Longitude Gradient Far Side	-999	20
perGreatArc(event)/f	degrees	Tangent Point Gradient Great Arc Change	-999	20

* f=float, d=double, s=short, i=int, c=char
** 04=1.04, 07=1.07, 20=2.0, RED means data unfilled for that version.
*** Description in Level1B files stating UT for this variable is incorrect

Table A.2 describes the contents of the SABER L2A files. This table lists each variable contained in the netCDF file along with its type, dimensions, units, long name, and missing value. The variables that are dimensioned use the variables: Altitude = 400, Event = UNLIMITED, and Vector =3. The Event dimension will depend on the number of events in the netCDF file. Vector is used only for a lunar vector variable. The variables that have the _top in the name are for the top half of the altitude range (extending to about 285km). The same variable without the _top extension is for the bottom half of the altitude range

(roughly 15km to 155km). Note that there are several versions of Level2A data, the column to the far right indicates for which versions (starting with 1.06) a particular variable is included.

Table A.2. Level 2A variables.

Variable(dimensions)/type*	units	Long name	Miss. value	Version**
event(event)/s		Event Number for Current File		06 07 20
date(event)/i	yyyyddd	Date [yyyyddd]	-999	06 07 20
mode(event)/s		0=Down 1=Up	-999	06 07 20
tpDN(event)/s		0=Day 1=Night 2=Twilight	-999	06 07 20
tpAD(event)/s		0=Ascending 1=Descending	-999	06 07 20
moonSepAngle(event)/f	degrees	Angle between moon and LOS	-999	06 07 20
tpaltmoonSepAngle(event)/f	km	Tpaltitude used for moonSepAngle	-999	06 07 20
solAP(event)/f		Solar Ap Index	-999	06 07 20
solKP(event)/f		Solar Kp Index	-999	06 07 20
solf10p7Daily(event)/f	10^{-22} W/m2/Hz	F10.7 Flux (Daily	-999	06 07 20
***solF10p781dAvg(event)/f	10^{-22} W/m2/Hz	F10.7 Flux (81-day Average)	-999	06 07 20
solSpotNo(event)/s		Zurich Sunspot Number	-999	06 07 20
scSolarZen(event)/f	degrees	Sc Solar-Zenith Angle	-999	06 07 20
earth_sun(event)/f	km	Earth-Sun Distance	-999	06 07 20
L1_altoff(event)/f	km	Altitude Offset from Level1	-999	-- -- 20
laurora(event)/s		Aurora Flag (1=TRUE, 0=FALSE)	-999	06 07 20
time(event,altitude)/i	msec	Msec Since Midnight	-999	06 07 20
sclatitude(event, altitude)/f	degrees	Spacecraft Latitude	-999	06 07 20
sclongitude(event, altitude)/f	degrees	Spacecraft Longitude	-999	06 07 20
scaltitude(event, altitude)/f	km	Spacecraft Altitude	-999	06 07 20
tpaltitude(event, altitude)/f	km	Tangent-Point Altitude	-999	06 07 20
tplatitude(event, altitude)/f	degrees	Tangent-Point Latitude	-999	06 07 20
tplongitude(event, altitude)/f	degrees	Tangent-Point Longitude	-999	06 07 20
tpSolarZen(event, altitude)/f	degrees	Tangent-Point Solar-Zenith Angle	-999	06 07 20
tpSolarLT(event, altitude)/f	msec	Tangent-Point Local-Solar Time	-999	06 07 20
elevation(event, altitude)/d	milliradians	Elevation Angle	-999	06 07 20
time_top/i	msec	Msec Since Midnight	-999	06 07 20
sclatitude_top(event,altitude)/f	degrees	Spacecraft Latitude	-999	06 07 20
sclongitude_top(event, altitude)/f	degrees	Spacecraft Longitude	-999	06 07 20
scaltitude_top(event,altitude)/f	km	Spacecraft Altitude	-999	06 07 20
tpaltitude_top(event,altitude)/f	km	Tangent-Point Altitude	-999	06 07 20
tplatitude_top(event,altitude)/f	degrees	Tangent-Point Latitude	-999	06 07 20

tplongitude_top(event,altitude)/f	degrees	Tangent-Point Longitude	-999	06 07 20
tpSolarZen_top(event,altitude)/f	degrees	Tangent-Point Solar-Zenith Angle"	-999	06 07 20
tpSolarLT_top(event,altitude)/f	msec	Tangent-Point Local-Solar Time	-999	06 07 20
elevation_top(event, altitude)/d	milliradians	Elevation Angle	-999	06 07 20
tpgpaltitude(event, altitude)/f	km	Tangent-Point Geopotential Altitude	-999	-- 07 20
pressure(event, altitude)/f	mbar	Pressure	-999	06 07 20
Pressure_error(event, altitude)/f	mbar	Pressure Error	-999	06 07 --
ktemp(event, altitude)/f	K	Kinetic Temperature (merge)	-999	06 07 20
ktemp_error(event, altitude)/f	K	Kinetic Temperature Error	-999	06 07 --
density(event, altitude)/f	$1/cm^3$	Atmospheric Density	-999	06 07 20
density_error(event, altitude)/f	$1/cm^3$	Atmospheric Density Error	-999	06 07 --
O3_96(event, altitude)/f	Mixing ratio	O3 Mixing Ratio 9.6µm	-999	06 07 20
O3_96_error(event, altitude)/f		O3 9.6µm channel Error	-999	06 07 --
O3_127(event, altitude)/f	Mixing ratio	O3 Mixing Ratio 1.27µm Channel	-999	06 07 20
O3_127_error(event, altitude)/f		O3 1.27µm channel Error	-999	06 07 --
H2O(event, altitude)/f	Mixing ratio	H2O Mixing Ratio	-999	06 07 20
H2O_error(event, altitude)/f		H2O Error	-999	06 07 --
CO2(event, altitude)/f	Mixing ratio	CO2 Mixing Ratio	-999	06 07 20
CO2_error(event, altitude)/f		CO2 Error	-999	06 07 --
O2_1sigma(event, altitude)/f	Mixing ratio	O2(1sigma) Mixing Ratio	-999	06 07 20
O(event, altitude)/f	Mixing ratio	O Mixing Ratio	-999	06 07 20
H(event, altitude)/f	Mixing ratio	H Mixing Ratio	-999	06 07 20
O2_1delta_ver(event, altitude)/f	$ergs/cm^3/sec$	O2(1delta) VER	-999	06 07 20
O2_1delta_ver_error(event, altitude)/f	$ergs/cm^3/sec$	O2(1delta) VER Error	-999	06 07 --
OH_16_ver(event, altitude)/f	$ergs/cm^3/sec$	OH VER for 1.6 µm Channel	-999	06 07 20
OH_16_ver_error(event, altitude)/f	$ergs/cm^3/sec$	OH VER Error	-999	06 07 --
OH_20_ver(event, altitude)/f	$ergs/cm^3/sec$	OH VER for 2.0 µm Channel	-999	06 07 20
OH_20_ver_error(event, altitude)/f	$ergs/cm^3/sec$	OH VER Error	-999	06 07 --
NO_ver(event, altitude)/f	$ergs/cm^3/sec$	NO VER	-999	06 07 20
NO_ver_top(event, altitude)/f	$ergs/cm^3/sec$	NO VER	-999	06 07 20

NO_ver_error(event, altitude)/f	ergs/cm^3/sec	NO VER Error	-999	06 07 --
NO_ver_top_error(event, altitude)/f	ergs/cm^3/sec	NO VER Error	-999	06 07 --
O2_1delta_ver_unfilt(event, altitude)/f	ergs/cm^3/sec	O2(1delta) VER	-999	06 07 20
O2_1delta_ver_unfilt_error(event, altitude)/f	ergs/cm^3/sec	O2(1delta) VER Error	-999	06 07 --
OH_16_ver_unfilt(event, altitude)/f	ergs/cm^3/sec	OH VER for 1.6 µm Channel	-999	06 07 20
OH_16_ver_unfilt_error(event, altitude)/f	ergs/cm^3/sec	OH VER Error	-999	06 07 --
OH_20_ver_unfilt(event, altitude)/f	ergs/cm^3/sec	OH VER for 2.0 µm Channel	-999	06 07 20
OH_20_ver_unfilt_error(event, altitude)/f	ergs/cm^3/sec	OH VER Error	-999	06 07 --
NO_ver_unfilt(event, altitude)/f	ergs/cm^3/sec	NO VER	-999	06 07 20
NO_ver_top_unfilt(event, altitude)/f	ergs/cm^3/sec	NO VER	-999	06 07 20
NO_ver_unfilt_error(event, altitude)/f	ergs/cm^3/sec	NO VER Error	-999	06 07 --
NO_ver_top_unfilt_error(event, altitude)/f	ergs/cm^3/sec	NO VER Error	-999	06 07 --

* f=float, d=double, s=short, i=int, c=char.

** 06=1.06, 07=1.07, 20=2.0, RED means data unfilled for that version.

*** The 81-day average F10.7 flux is not available because the 81-day average is centered about the current day; while we could run on older data and have a value, processing of the newer data would have to be delayed until +40 days after the date of the data to permit the average value to be calculated. The daily flux value (limited to the range 71 - 212) is substituted for the average in the processing code.

Table A.3 describes the contents of the SABER L2B files. This table lists each variable contained in the netCDF file along with its type, dimensions, units, long name, and missing value. The variables that are dimensioned use the variables: Altitude = 400, Event = UNLIMITED, and Vector =3. The Event dimension will depend on the number of events in the netCDF file. Vector is used only for a lunar vector variable. The variables that have the _top in the name are for the top half of the altitude range (extending to about 285km). The same variable without the _top extension is for the bottom half of the altitude range (roughly 15km to 155km). Note that there are several versions of Level2B data, the column to the far right indicates for which versions (starting with 1.06) a particular variable is included.

Table A.3. Level 2B variables.

Variable(dimensions)/type*	units	Long name	Miss. value	Version**
event(event)/s		Event Number for Current File		06 07 20
date(event)/i	yyyyddd	Date [yyyyddd]	-999	06 07 20
mode(event)/s		0=Down 1=Up	-999	06 07 20

tpDN(event)/s		0=Day 1=Night 2=Twilight	-999	06 07 20
tpAD(event)/s		0=Ascending 1=Descending	-999	06 07 20
moonSepAngle(event)/f	degrees	Angle between moon and LOS	-999	06 07 20
tpaltmoonSepAngle(event)/f	km	Tpaltitude used for moonSepAngle	-999	06 07 20
solAP(event)/f		Solar Ap Index	-999	06 07 20
solKP(event)/f		Solar Kp Index	-999	06 07 20
solf10p7Daily(event)/f	10^{-22} W/m2/Hz	F10.7 Flux (Daily	-999	06 07 20
***solF10p781dAvg(event)/f	10^{-22} W/m2/Hz	F10.7 Flux (81-day Average)	-999	06 07 20
solSpotNo(event)/s		Zurich Sunspot Number	-999	06 07 20
scSolarZen(event)/f	degrees	Sc Solar-Zenith Angle	-999	06 07 20
earth_sun(event)/f	km	Earth-Sun Distance	-999	06 07 20
L1_altoff(event)/f	km	Altitude Offset from Level1	-999	-- -- 20
laurora(event)/s		Aurora Flag (1=TRUE, 0=FALSE)	-999	06 07 20
time(event,altitude)/i	msec	Msec Since Midnight	-999	06 07 20
sclatitude(event, altitude)/f	degrees	Spacecraft Latitude	-999	06 07 20
sclongitude(event, altitude)/f	degrees	Spacecraft Longitude	-999	06 07 20
scaltitude(event, altitude)/f	km	Spacecraft Altitude	-999	06 07 20
tpaltitude(event, altitude)/f	km	Tangent-Point Altitude	-999	06 07 20
tplatitude(event, altitude)/f	degrees	Tangent-Point Latitude	-999	06 07 20
tplongitude(event, altitude)/f	degrees	Tangent-Point Longitude	-999	06 07 20
tpSolarZen(event, altitude)/f	degrees	Tangent-Point Solar-Zenith Angle	-999	06 07 20
tpSolarLT(event, altitude)/f	msec	Tangent-Point Local-Solar Time	-999	06 07 20
elevation(event, altitude)/d	milliradians	Elevation Angle	-999	06 07 20
NO_cool(event, altitude)/f	K/day	cooling rate for NO	-999	06 07 --
CO2_cool_626_01101_00001(event, altitude)/f	K/day	cooling rate for CO2_626_01101_00001	-999	06 07 20
CO2_cool_626_02201_01101(event, altitude)/f	K/day	cooling rate for CO2_626_02201_01101	-999	06 07 20
CO2_cool_626_03301_02201(event, altitude)/f	K/day	cooling rate for CO2_626_03301_02201	-999	06 07 20
CO2_cool_626_00011_00001(event, altitude)/f	K/day	cooling rate for CO2_626_00011_00001	-999	06 07 20
CO2_cool_626_01111_01101(event, altitude)/f	K/day	cooling rate for CO2_626_01111_01101	-999	06 07 20
CO2_cool_626_10012_00001(event, altitude)/f	K/day	cooling rate for CO2_626_10012_00001	-999	06 07 20
CO2_cool_626_10011_00001(event, altitude)/f	K/day	cooling rate for CO2_626_10011_00001	-999	06 07 20
CO2_cool_626_10012_10002(event, altitude)/f	K/day	cooling rate for CO2_626_10012_10002	-999	06 07 20
CO2_cool_626_02211_02201(event, altitude)/f	K/day	cooling rate for CO2_626_02211_02201	-999	06 07 20
CO2_cool_626_10011_10001(event, altitude)/f	K/day	cooling rate for CO2_626_10011_10001	-999	06 07 20

CO2_cool_626_11112_01101(event, altitude)/f	K/day	cooling rate for CO2_626_11112_01101	-999	06 07 20
CO2_cool_626_11111_01101(event, altitude)/f	K/day	cooling rate for CO2_626_11111_01101	-999	06 07 20
CO2_cool_626_11112_11102(event, altitude)/f	K/day	cooling rate for CO2_626_11112_11102	-999	06 07 20
CO2_cool_626_03311_03301(event, altitude)/f	K/day	cooling rate for CO2_626_03311_03301	-999	06 07 20
CO2_cool_626_11111_11101(event, altitude)/f	K/day	cooling rate for CO2_626_11111_11101	-999	06 07 20
CO2_cool_626_20013_00001(event, altitude)/f	K/day	cooling rate for CO2_626_20013_00001	-999	06 07 20
CO2_cool_626_20012_00001(event, altitude)/f	K/day	cooling rate for CO2_626_20012_00001	-999	06 07 20
CO2_cool_626_20011_00001(event, altitude)/f	K/day	cooling rate for CO2_626_20011_00001	-999	06 07 20
CO2_cool_636_01101_00001(event, altitude)/f	K/day	cooling rate for CO2_636_01101_00001	-999	06 07 20
CO2_cool_636_02201_01101(event, altitude)/f	K/day	cooling rate for CO2_636_02201_01101	-999	06 07 20
CO2_cool_636_00011_00001(event, altitude)/f	K/day	cooling rate for CO2_636_00011_00001	-999	06 07 20
CO2_cool_628_01101_00001(event, altitude)/f	K/day	cooling rate for CO2_628_01101_00001	-999	06 07 20
CO2_cool_628_02201_01101(event, altitude)/f	K/day	cooling rate for CO2_628_02201_01101	-999	06 07 20
CO2_cool_628_00011_00001(event, altitude)/f	K/day	cooling rate for CO2_628_00011_00001	-999	06 07 20
CO2_cool_627_01101_00001(event, altitude)/f	K/day	cooling rate for CO2_627_01101_00001	-999	06 07 20
CO2_cool_627_02201_01101(event, altitude)/f	K/day	cooling rate for CO2_627_02201_01101	-999	06 07 20
CO2_cool_627_00011_00001(event, altitude)/f	K/day	cooling rate for CO2_627_00011_00001	-999	06 07 20
H2O_cool_161_010_000(event, altitude)/f	K/day	cooling rate for H2O_161_010_000	-999	06 07 20
H2O_cool_161_020_000(event, altitude)/f	K/day	cooling rate for H2O_161_020_000	-999	06 07 20
H2O_cool_161_020_010(event, altitude)/f	K/day	cooling rate for H2O_161_020_010	-999	06 07 20
H2O_cool_161_100_000(event, altitude)/f	K/day	cooling rate for H2O_161_100_000	-999	06 07 20
H2O_cool_161_100_010(event, altitude)/f	K/day	cooling rate for H2O_161_100_010	-999	06 07 20
H2O_cool_161_001_000(event, altitude)/f	K/day	cooling rate for H2O_161_001_00	-999	06 07 20

H2O_cool_161_001_010(event, altitude)/f	K/day	cooling rate for H2O_161_001_010	-999	06 07 20
H2O_cool_161_011_000(event, altitude)/f	K/day	cooling rate for H2O_161_011_000	-999	06 07 20
H2O_cool_farir(event,altitude)/f	K/day	cooling rate for H2O in the far-ir	-999	06 07 --
O3_cool_666_001_000(event, altitude)/f	K/day	cooling rate for O3_666_001_000	-999	06 07 20
O3_cool_666_010_000(event, altitude)/f	K/day	cooling rate for O3_666_010_000	-999	06 07 --
O3_cool_666_100_000(event, altitude)/f	K/day	cooling rate for O3_666_100_000	-999	06 07 --
O3_cool_666_011_001(event, altitude)/f	K/day	cooling rate for O3_666_011_001	-999	06 07 --
CO2_solar_heat_626_00011_00001(event, altitude)/f	K/day	solar_energy deposition rate for CO2_626_00011_00001	-999	06 07 --
CO2_solar_heat_626_01111_01101(event, altitude)/f	K/day	solar_energy deposition rate for CO2_626_01111_01101	-999	06 07 --
CO2_solar_heat_626_10012_00001(event, altitude)/f	K/day	solar_energy deposition rate for CO2_626_10012_00001	-999	06 07 --
CO2_solar_heat_626_10011_00001(event, altitude)/f	K/day	solar_energy deposition rate for CO2_626_10011_00001	-999	06 07 --
CO2_solar_heat_626_10012_10002(event, altitude)/f	K/day	solar_energy deposition rate for CO2_626_10012_10002	-999	06 07 --
CO2_solar_heat_626_02211_02201(event, altitude)/f	K/day	solar_energy deposition rate for CO2_626_02211_02201	-999	06 07 --
CO2_solar_heat_626_10011_10001(event, altitude)/f	K/day	solar_energy deposition rate for CO2_626_10011_10001	-999	06 07 --
CO2_solar_heat_626_11112_01101(event, altitude)/f	K/day	solar_energy deposition rate for CO2_626_11112_01101	-999	06 07 --
CO2_solar_heat_626_11111_01101(event, altitude)/f	K/day	solar_energy deposition rate for CO2_626_11111_01101	-999	06 07 --
CO2_solar_heat_626_11112_11102(event, altitude)/f	K/day	solar_energy deposition rate for CO2_626_11112_11102	-999	06 07 --
CO2_solar_heat_626_03311_03301(event, altitude)/f	K/day	solar_energy deposition rate for CO2_626_03311_03301	-999	06 07 --
CO2_solar_heat_626_11111_11101(event, altitude)/f	K/day	solar_energy deposition rate for CO2_626_11111_11101	-999	06 07 --
CO2_solar_heat_626_20013_00001(event, altitude)/f	K/day	solar_energy deposition rate for CO2_626_20013_00001	-999	06 07 --
CO2_solar_heat_626_20012_00001(event, altitude)/f	K/day	solar_energy deposition rate for CO2_626_20012_00001	-999	06 07 --
CO2_solar_heat_626_20011_00001(event, altitude)/f	K/day	solar_energy deposition rate for CO2_626_20011_00001	-999	06 07 --
CO2_solar_heat_636_00011_00001(event, altitude)/f	K/day	solar_energy deposition rate for CO2_636_00011_00001	-999	06 07 --
CO2_solar_heat_628_00011_00001(event, altitude)/f	K/day	solar_energy deposition rate for CO2_628_00011_00001	-999	06 07 --

CO2_solar_heat_627_00011_00001(event, altitude)/f	K/day	solar_energy deposition rate for CO2_627_00011_00001	-999	06 07 --
H2O_solar_heat_161_010_000(event, altitude)/f	K/day	solar_energy deposition rate for H2O_161_010_000	-999	06 07 --
H2O_solar_heat_161_020_000(event, altitude)/f	K/day	solar_energy deposition rate for H2O_161_020_000	-999	06 07 --
H2O_solar_heat_161_020_010(event, altitude)/f	K/day	solar_energy deposition rate for H2O_161_020_010	-999	06 07 --
H2O_solar_heat_161_100_000(event, altitude)/f	K/day	solar_energy deposition rate for H2O_161_100_000	-999	06 07 --
H2O_solar_heat_161_100_010(event, altitude)/f	K/day	solar_energy deposition rate for H2O_161_100_010	-999	06 07 --
H2O_solar_heat_161_001_000(event, altitude)/f	K/day	solar_energy deposition rate for H2O_161_001_000"	-999	06 07 --
H2O_solar_heat_161_001_010(event, altitude)/f	K/day	solar_energy deposition rate for H2O_161_001_010	-999	06 07 --
H2O_solar_heat_161_011_000(event, altitude)/f	K/day	solar_energy deposition rate for H2O_161_011_000	-999	06 07 --
SJ_hartley(event, altitude)/f	/s	Photodissociation rate for O3_hartley	-999	-- -- 20
O3_solar_heat_hartley(event, altitude)/f	K/day	solar heating rate for O3_hartley	-999	06 07 20
O3_solar_heat_huggins(event, altitude)/f	K/day	solar heating rate for O3_huggins	-999	06 07 20
O3_solar_heat_chappuis(event, altitude)/f	K/day	solar heating rate for O3_chappuis	-999	06 07 20
O2_solar_heat_ly_alpha(event, altitude)/f	K/day	solar heating rate for O2_ly_alpha	-999	06 07 20
O2_solar_heat_herzberg(event, altitude)/f	K/day	solar heating rate for O2_herzberg	-999	06 07 20
O2_solar_heat_schumann_runge_cont(event, altitude)/f	K/day	solar heating rate for O2_schumann_runge_cont	-999	06 07 20
O2_solar_heat_schumann_runge_band(event, altitude)/f	K/day	solar heating rate for O2_schumann_runge_band	-999	06 07 20
O2_solar_heat_atmospheric_bands(event, altitude)/f	K/day	solar energy deposition rate O2_atmospheric_bands	-999	06 07 20
chem_heat_H_O2_M(event, altitude)/f	K/day	chemical heating rate for H+O2+M	-999	06 07 20
chem_heat_H_O3(event, altitude)/f	K/day	chemical heating rate for H+O3	-999	06 07 20
chem_heat_O_O3(event, altitude)/f	K/day	chemical heating rate for O+O3	-999	06 07 20
chem_heat_O_OH(event, altitude)/f	K/day	chemical heating rate for O+OH	-999	06 07 20
chem_heat_O_HO2(event, altitude)/f	K/day	chemical heating rate for O+HO2	-999	06 07 20
chem_heat_O_O_M(event, altitude)/f	K/day	chemical heating rate for O+O+M	-999	06 07 20

chem_heat_O_O2_M(event, altitude)/f	K/day	chemical heating rate for O+O2+M	-999	06 07 20

* f=float, d=double, s=short, i=int, c=char.

** 06=1.06, 07=1.07, 20=2.0, RED means data unfilled for that version.

*** The 81-day average F10.7 flux is not available because the 81-day average is centered about the current day; while we could run on older data and have a value, processing of the newer data would have to be delayed until +40 days after the date of the data to permit the average value to be calculated. The daily flux value (limited to the range 71 - 212) is substituted for the average in the processing code.